International Journal of Fatigue 143 (2021) 106004

Contents lists available at ScienceDirect

International Journal of Fatigue

journal homepage: www.elsevier.com/locate/ijfatigue

Fatigue endurance limit and crack front evolution in metallic glass

Xianqi Lei [a], Lichao Yuan [a], Liu Peng [b], Chengqi Sun [a], Bingchen Wei [a], Yujie Wei [a,*]

[a] LNM, Institute of Mechanics, Chinese Academy of Sciences, Beijing 100190, PR China
[b] National Center for Materials Service Safety, University of Science and Technology Beijing, Beijing 100083, PR China

ARTICLE INFO

Keywords:
Fatigue endurance limit
Ultra-high cycle fatigue
Metallic glasses
Elliptical crack front
Stress intensity factor

ABSTRACT

Fatigue endurance limit is a threshold stress-amplitude under which a solid subjected to a cyclic loading can sustain infinite life. Such a limit has been confirmed in ferrous materials but remains controversial in many advanced new materials, including bulk metallic glasses with superb strength. By using a combination of ultrasonic fatigue (USF) test and conventional fatigue test, we obtain the stress amplitude vs. loading cycle curve of the Vitreloy 1^{TM} metallic glass, with loading cycles up to 10^9. There is a clear fatigue endurance limit (FEL) which is about 320 MPa, and is 17% of the strength of Vitreloy 1^{TM}. The residual strength of survivals after 10^9 cycles is nearly the same as those of intact samples. We demonstrate that all fatigue cracks initiate from spherical pores which are inevitable and intrinsic amid casting and fast cooling, and the fatigue crack front resembles an ellipse arc till final rapid rapture of all tested samples. The size and position of a pore can be utilized to extract the fatigue initiation threshold K_0^{th}, and the elliptical fatigue crack front is used to obtain the mode I fracture toughness K_{IC}, which are $K_0^{th} = 2.0 \pm 0.5\text{MPa}\sqrt{\text{m}}$ and $K_{IC} = 18 - 20\text{MPa}\sqrt{\text{m}}$ for Vitreloy 1^{TM}, respectively. The fatigue endurance limit and its intrinsic origin of Vitreloy 1^{TM} pave the way to understand fatigue in other metallic glasses.

1. Introduction

Fatigue is the progressive, localized and permanent structural change accumulated in materials when they are subjected to cyclic strain or stress at levels lower than their yield strength [1]. Cycle by cycle, localized plastic deformation accumulates and triggers micro-cracks (stage I); these micro-cracks may then start to grow and propagate steadily (stage II), and end up with fast fracture (stage III). The applied stress amplitude (S) vs cycles (N), known as an S-N curve, is usually used to describe the fatigue properties of materials. The largest stress amplitude under which fatigue failure does not occur, the horizontal asymptote of stress of an S-N curve, is the fatigue endurance limit (FEL) of the material [2]. The FEL is one of the most significant material properties, and of great practical interest for many engineering structures subject to fatigue failure. We may mathematically define S_{EL} an FEL which a material may survive infinite number of cycles without fatigue for stress amplitudes below this level. In engineering practice, it is often determined if the material can sustain a sufficiently large number of cycles N_f at S_{EL}. In convention, a broadly used cut-off number is 10^7 and we define a pseudo FEL if the material subjected to S_{EL} can survive $N_{f0} = 10^7$ cycles. It does not guarantee however, the materials are fatigue-proof if loading cycles may be greater than N_{f0}. Indeed, many alloys of both FCC and FCC lattice show a decrease in fatigue strength at cycle numbers greater than N_{f0} [3,4]. Consequently, it raises grand challenges for engineering practices as nowadays structures are designed for safety after cycles of 10^9 or even higher.

In polycrystalline fields, understanding FEL and micro-cracks initiation have been a long-lasting research. Models basing on dislocation pile up at grain boundaries for fatigue crack initiation [5] and empirical formula correlating the fatigue endurance limit with the square root of the defect projection area [6] had been proposed in the early 1980 s. Creative thermographic methodology and energy dissipation strategies [7,8], effect of inclusion in subsurface crack initiation [9], influence of defect geometry on fatigue limit [10], persistent slip bands structure energy based crack initiation criterion [11], formation of discontinuous gradient regimes [12] had all been explored. Progress on this respect has been critically reviewed, unified and documented for engineering practices. Effects of defects, inclusions and inhomogeneity on fatigue strength of materials [13–17], fatigue of materials and structures [2], roles of microstructure in fatigue crack initiation [3,18], models of fatigue endurance limit under multiaxial loading [19], notches and residual stresses on fatigue mechanisms [4], text books [20], perspectives

* Corresponding author.
E-mail address: yujie_wei@lnm.imech.ac.cn (Y. Wei).

https://doi.org/10.1016/j.ijfatigue.2020.106004
Received 28 June 2020; Received in revised form 29 September 2020; Accepted 18 October 2020
Available online 22 October 2020

[21] and guide lines for defected material fatigue design [22] had been reported and published.

In the past two decades, the appearance of bulk metallic glasses (BMGs) attracts the attention of researchers for their high strength, superior elastic limit, high toughness, and good corrosion resistance [23–26]. MGs are significantly different from polycrystalline materials due to lacking of long-range orders, and they have an intrinsic inotropic critical dimension at tens of nanometers [27], which are about orders of magnitude lower than that of traditional polycrystalline materials.

As a corollary, MGs exhibit distinct fatigue behavior in contrast to their polycrystalline counterparts. Gilbert et al. were the first ones to explore fatigue behavior of BMGs [28,29]. Their four-point-bending fatigue experiments with Vitreloy 1^{TM}, with the conventional definition of FEL for surviving $N_{f0} = 10^7$ cycles, leaded to an ultra-low FEL which S_{EL} is only about ~8% of σ_y – the tensile strength of Vitreloy 1^{TM}. Menzel and Dauskardt reported similar experimental investigation and S_{EL} is about ~10% of σ_y [30]. Yue et al obtained a rather high FEL, which is about 34% of σ_y for Vitreloy 1^{TM} when the sample is subjected to cyclic tension, and corresponding FEL from their three-point bending drops to 12% of σ_y [31]. Wang et al, in contrast, found an FEL of ZT3 ($Ti_{32.8}Zr_{30.2}Ni_{15.3}Cu_9Be_{22.7}$, atom%) using three-point bending to be ~29% of σ_y [32]. Fujita et al. carried out fatigue tests on ultra-high strength Co- and Fe-based BMGs and reported FELs close to ~50% of their respective strength [33]. Yokoyama et al., by adding small amount noble elements in Zr-Cu-Al based BMGs, reported enhanced FEL up to 55% of their respective strength [34]. Except the conventional fatigue experiments mentioned above, there are also in situ experiments [35] and simulation [36,37] focusing on FEL of BMGs. For a comprehensive review, the readers are referred to the reference by Jia et al. [38].

Regardless the tremendous progress on research for FEL of BMGs, there are two critical issues which require close examination: (1) The extension of endurance limit beyond $N_{f0} = 10^7$. So far most of the research missed the connection to define an FEL, based on consistent experiments, extending from the conventional limit cycle number $N_{f0} = 10^7$ to 10^9 or even higher; and (2) No close examination on the intrinsic defects origin of FEL in BMGs which may be resulted from manufacturing. To fill the gap and address those two important issues for potential engineering applications of BMGs, we investigate in this paper the fatigue performance of Vitreloy 1^{TM} using both conventional and ultra-sonic fatigue tests to cycles ranging from 10^4 to 10^9.

2. Experiments

We use the well investigated metallic glass Vitreloy 1^{TM} ($Zr_{41}Ti_{14}Cu_{12.5}Ni_{10}Be_{22.5}$, atom%). The material is prepared in a water-cooled arc-melting hearth under titanium-gathered argon atmosphere. Elemental metals (>99.9% purity) are used to form the master alloy and suction-casted into cylinders of 8 mm in diameter. Those cylinders were then machined and polished to finish-up the dog-bone samples with dimensions shown in Fig. 1. The samples tested using ultrasonic fatigue (USF) are shown in Fig. 1a and b, and they have an axial vibration modal frequency of 20 KHz given the Young's modulus of $E = 100$ GPa and Poisson's ratio $\nu = 0.35$. The USF tests are conducted using a Shimadzu USF2000. A resonant frequency of 20 KHz and R ratio of −1 are applied, where $R = \sigma_{min}/\sigma_{max}$, for σ_{min} and σ_{max} the minimum and the maximum stresses during a stress cycle, respectively. A final experimental setup is shown in Fig. 1c. As the system is under displacement control, the stress amplitudes are calculated and calibrated based on the elastic response of the real sample shown in Fig. 1a. The fatigue life N_f of each sample is recorded if fatigue fracture occurs before 10^9 cycles. Samples tested at different stress amplitude may then lead to two final statuses: (1) fracture due to fatigue, and the fractography is characterized by using a FEI Sirion SEM; (2) survive after 10^9 cycles, we consider them to have an 'infinite' life time, and apply tensile tests to obtain their residual strength after 10^9 cyclic loading. Conventional fatigued (MTS) tests using a servo-hydraulic MTS test system (Fig. 1d–f). A sinusoidal wave format at 30 Hz frequency, R ratio −1 and loads control method are selected to conduct the tests until the samples fail. The sample dimensions, applied loads, fatigue failure life, and residual strength for both the USF and MTS tests are all listed as in Table 1.

3. Results and discussion

3.1. The S-N curve of vitreloy 1^{TM}

The stress amplitudes and corresponding cycles from both USF and MTS tests are plotted in Fig. 2a. It can be seen that the both datasets in

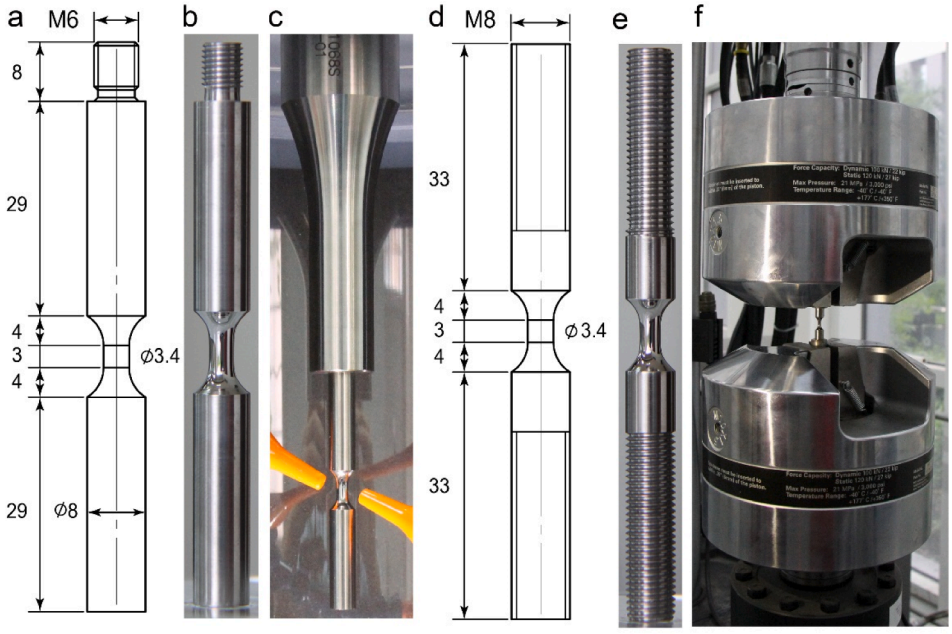

Fig. 1. Sample designs and fatigue test set ups. (a)–(c) Sample dimension, layout and experimental setup for ultrasonic fatigue tests; (d)–(f) Sample dimenson, layout and experimental setup for conventional fatigue (MTS) tests.

Table 1
Detailed information about samples for ultrasonic fatigue test using USF and conventional fatigue tests with MTS. The applied stress amplitude S_a, faliure cycle N_f, residual strength σ_{RS} for samples of "infinite life", sample radius R at the guaged section, pore position d, pore radius r, half short axis a_c and half long axis b_c of the ellipitical fracture front, and the maximum nomal stress intensitor factor K_0 (normalized by $\sigma_\infty\sqrt{\pi r}$, for σ_∞ being the nominal stress, the applied loading divided by the fractured cross-section of the sample). Sample tested with MTS are identified by a superscript "*".

No.	S_a(MPa)	N_f(cycle)	σ_{RS}(MPa)	$2R$(mm)	$2d(\mu m)$	$2r(\mu m)$	a_c(mm)	b_c(mm)	R/r	d/r	$K_0\sigma_\infty\sqrt{\pi r}$
1*	488	2.06×10^4	/	3.23	34	34.8	1.61	2.273	93	0.98	1.15
2*	433	2.80×10^4	/	3.34	10	10.0	0.50	0.594	300	1.00	1.18
3*	385	5.00×10^4	/	3.35	32	40.2	0.70	0.828	85	0.80	1.03
4*	365	5.50×10^4	/	3.33	11	12.5	1.00	1.276	267	0.88	1.10
5	481	7.81×10^4	/	2.50	0	25.8	1.40	2.659	97	0	0.80
6	481	5.62×10^4	/	2.50	0	93.2	0.96	1.084	27	0	0.80
7	341	7.12×10^4	/	3.26	15.0	15.0	1.17	1.416	217	1.00	1.18
8	343	7.81×10^4	/	3.28	23.6	25.6	0.85	1.118	128	0.92	1.13
9	414	9.66×10^4	/	2.50	12.0	12.0	1.80	3.528	208	1.00	1.18
10	331	3.12×10^7	/	3.42	6.00	7.78	1.81	3.528	440	0.77	0.98
11	333	7.68×10^4	/	3.31	20.0	22.9	1.50	2.520	145	0.87	1.08
12	321	1.14×10^6	/	3.36	16	20	1.13	1.532	118	0.80	1.03
13	324	6.93×10^8	/	3.26	7.20	7.20	1.20	1.761	450	1.00	1.18
14	319	1.09×10^5	/	3.24	24.7	29.7	0.75	0.907	109	0.83	1.05
15*	300	$>5\times10^5$	1769	3.40	/	/	/	/	/	/	/
16*	320	$>10^7$	1869	3.26	/	/	/	/	/	/	/
17*	330	$>10^7$	1964	3.30	/	/	/	/	/	/	/
18*	342	$>5\times10^5$	1824	3.34	/	/	/	/	/	/	/
19*	350	$>5\times10^5$	1769	3.30	/	/	/	/	/	/	/
20	318	$>10^9$	1899	3.21	/	/	/	/	/	/	/
21	324	$>2\times10^8$	1903	3.24	/	/	/	/	/	/	/
22	329	$>10^9$	1907	3.25	/	/	/	/	/	/	/
23*	/	/	1891	3.94	/	/	/	/	/	/	/

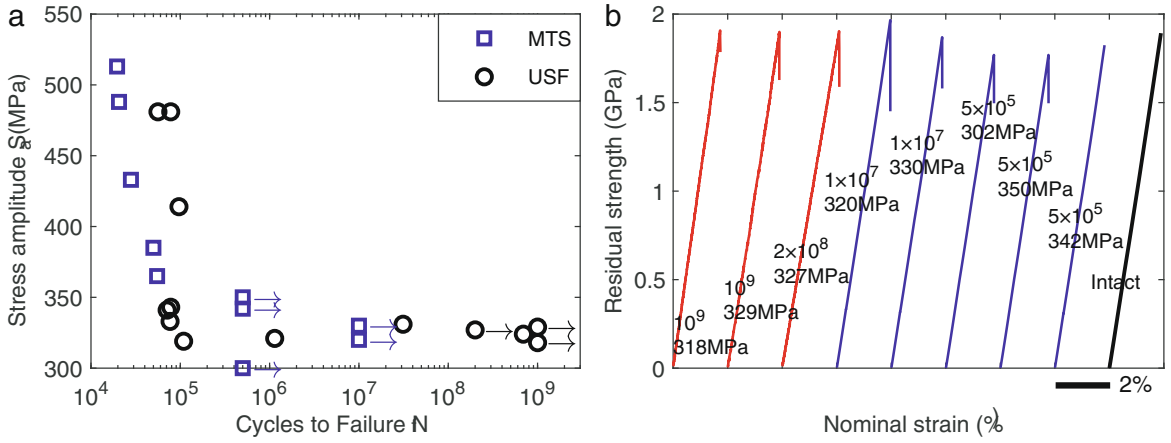

Fig. 2. The fatigue properties of Vitreloy 1^{TM}: (a) the *S-N* curve, both Ultrasonic fatigue tests ($N_f > 10^7$) and conventional fatigue tests (MTS) ($N_f \leq 10^7$) are shown. (b) The stress–strain curve of samples survived a certain number of cyclic loading, from which we extract the residual strength of cyclically loaded samples.

combination lead to a consistent and convincing conclusion that there is a fatigue endurance limit in Vitreloy 1^{TM}. Despite the 2 to 3 orders of magnitude difference in loading frequency for USF tests and MTS tests, 20 KHz and 10–30 Hz respectively, both testing methods lead to an FEL S_{el} about 320 MPa. The application of USF tests in metallic glass enables us to reach a fatigue cycles on the order of 10^9 10^{10}, which is of significance in engineering practice for very-high cycle fatigue applications. It is noted that FEL is about 17% of its strength σ_y of Vitreloy 1^{TM}.

To examine the potential impact of cyclic loading on the strength of BMG samples, we further conduct tensile tests to those samples survived the infinite fatigue life test (beyond 10^9 cycles) and see whether there is any strength degradation. The stress and strain curves of those samples are plotted in Fig. 2b. From the initial linear region, It can be seen that after 10^9 cycles of loading, the stress–strain curves keep linear and there is no elastic degradation. This may suggest that cyclic loading with stress amplitude below S_{el} does not introduce internal structural change in those BMG samples. After loading of 10^7 and 10^9 cycles, the samples exhibiting 'infinite life time' have an residual strength of 1861 ± 70 MPa, which is about the same as the ultimate tensile strength of ~1900 MPa of as-received samples. We summarize in Table 1 information of all samples and their experimental results.

As note above, the limited reports about the fatigue endurance limit ratio of BMGs are very scattering, from 8% to 55% [38]. The big discrepancy may result from factors such as experiments method (bending, compact tension, tension, tension compression, compression and specific fatigue ratio R), sample goemetry (especially notched or

not, and pre-crack or not), material state (relaxation free volume, residual stress and oxygen content ppm) [26,28–31,39,40]. Schuh et al. reviewed and suggested that residual stresses and structural relaxation should be important intrinsic factors accounting for the FEL of BMGs [26,38]. We further identified here that fatigue crack emanating from microsized pores, which is intrinsic during the synthesize of BMG samples, governs the FEL of BMGs.

3.2. Fractography of fatigued samples

Knowing the governing mechanisms associated with fatigue fracture is of significance for better life assessment and clues for materials design for better resistance to fatigue failure. Dauskardt et al. [41], based on free volume mechanism, explored crack-growth rate and defects evolution monitoring in metallic glass. We examine closely the fractography of fatigue failured samples, as shown in Fig. 3. It can be seen from Fig. 3a that a typical fracture surface can be divided into three zones: the initiation zone, the propagation zone and the fast fracture zone. Unlike early reports, we found it invariable that a fatigue crack initiates from a spherical pore with diameters on the order of 10 μm, as shown in Fig. 3b and f for two distinct samples. The pore size responsible for fatigue initiation in all fatigued samples are measured and summarized in Table 1. In the extending zone, typical striations can be seen (Fig. 3c, g), and which is widely accepted that striations spacings have a relationship with its local stress intensity factor. At the end of the extending zone is the boundary for the beginning of fast fracture zone, and the sample breaks apart abruptly, and the stress intensity factor characterized by this fracture line is related to the fatigue fracture toughness of the material.

It is noted that early works [30] did mentioned the existence and potential impact of pore defects to fatigue. For convenience, many early works use standard compact tension (CT), three-point bending (3 PB) [42], four-point bending (4 PB), and notched samples with prefabricated defects [43] to study the fatigue properties of metallic glasses. Those artificial defects are usually larger in dimension than natural pores found here. Most likely, such prefabricated defects will interrupt and blur the natural fatigue crack initiation process that usually happen in engineering service. For metallic glass, the form of this kind of spherical pores about tens of micrometer in size should be natural and intrinsic. Such characteristics make it easy to build standard model for fatigue mechanisms in BMGs.

3.3. Stress intensity factor for crack initiation

Since a crack initiates from a spherical pore near the sample surface, it is of interest to evaluate the crack initiation intensity factor K_0 around the pores and the influence of geometrical factors like the position and the size of the pore. In Fig. 4a, we illustrate a sample whose radius at the gauged section is R, and the radius of a spherical pore is r, the distance between the pore center and sample edge is difined as d. Depending on d/r, the relative postion of the pore in the sample may be categorized into three scenarios, as illistrated in Fig. 4a. We particularly mark two points, the arc apex point "A" and the opposite point "B" for late reference, as illustrated in Fig. 4a for $R \gg r$, and that is the case in our tests (Table 1).

Liner elastic finite element simulations are employed to evalute the stress intensity factors accounting for crack initiation from pores [44]. Material parameters include the Young's modulus and Poison's ratio, which are E = 100GPa and ν = 0.35, respectively. Following the instructions by the commercial software (Abaqus 6.14) [45], a convergent J-integral around the 'pore-like' crack can be obtained for a sufficiently large contour zone. For a special case while the pore locates at the center of the sample, as illustrated in Fig. 4b and the tension is applied along the Z-axis. The equator line of the pore (O-E-E' as illustrated) is the

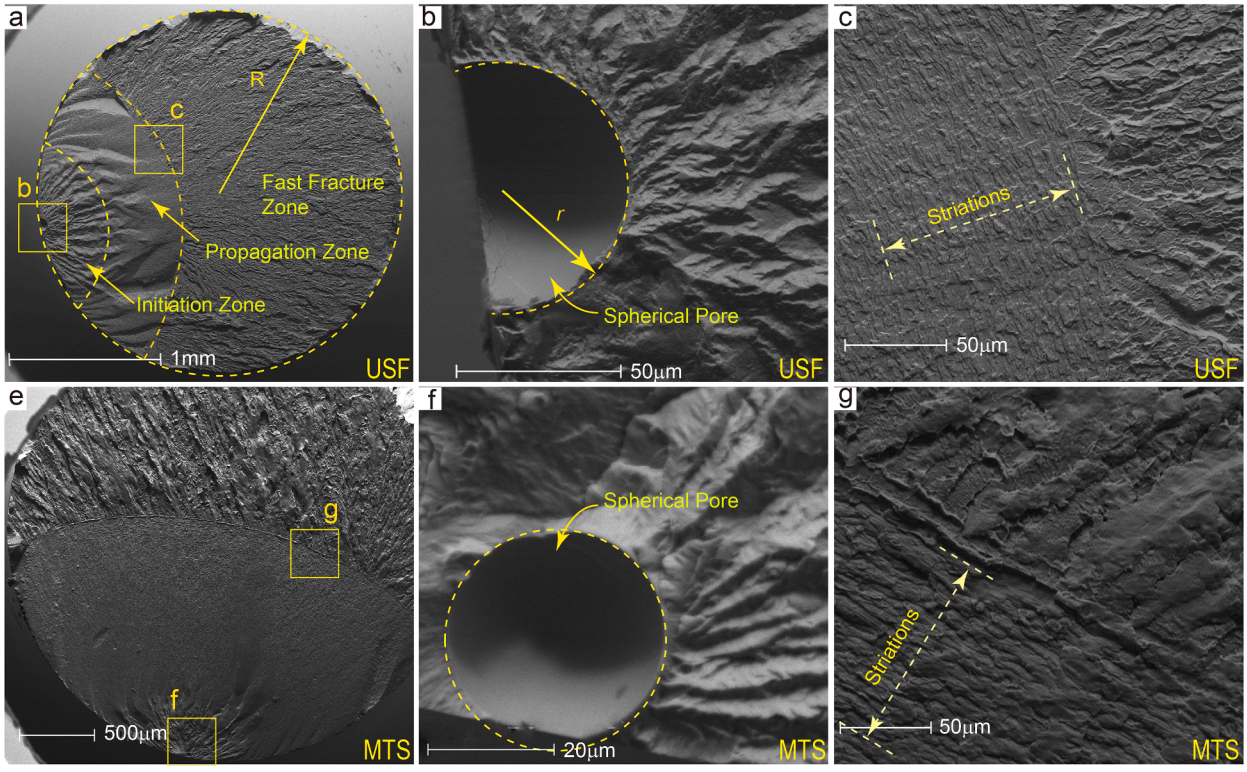

Fig. 3. Fractographies of fatigued samples tested. (a)–(c), results from UTS samples, (a) Fatigue crack propagation in Vitreloy 1^{TM} can be divided into three distinct zones: initiation zone, propagation zone and fast fracture zone; (b) A close-up to show the initiation zone from a spherical pore; (c) High resolution view in the propagation zone to show striations. (e)–(g), results from the MTS counter test, (e) the three distinct zones, (f) the cavity where crack initiates, (g) The striation left behind as fatigue crack propagate.

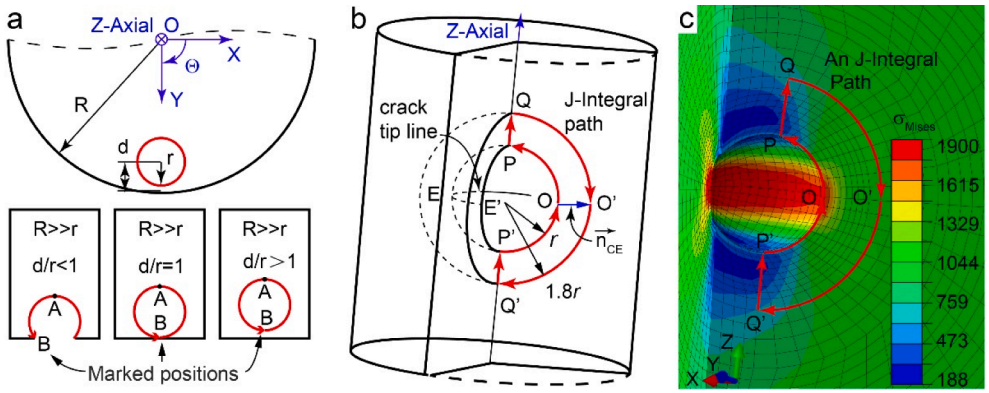

Fig. 4. Illustration to show the relative position of the pore and the J-integral path for stress intensity factor calculations in the FEM model. (a) cross-section where the equatorial cycle of the pore resides, radius R of the cross section, pore position d and pore radius r, and three typical positons of pores with $d/r < 1$, $d/r = 1$ and $d/r > 1$. Along the equatorial line of the pore in the crack plane, we mark the inner most arc apex point as 'A', and the out most arc boundary point as 'B' for later reference; (b) Illustration to show an J-integral path O-P-Q-O′-Q′-P′-O for an embedded pore-like crack. (c) the von Mises stress contour around the 'crack front' zone using a sample with $d/r = 0.8$, R/r = 80 and $\sigma_\infty = 1000$MPa.

'crack tip line', hence Z-axis is the normal of the potential crack plane defined by the crack-tip line. The outer normal $\vec{n}_{CE}$ of the 'crack tip line' is the crack extension direction. The loop O-P-Q-O′-Q′-P′-O shown in Fig. 4b is a typical J-Integral path. By rotating the loop O-P-Q-O′-Q′-P′-O with respect to the polar axis of the pore – the line passing the pore center and in the Z-direction, we obtain the J-Integral path at any point along the 'crack tip line' and obtain the corresponding J-integral. It is also noted that the 'crack front' zone are meshed using three-dimensional brick elements (C3D8R) in Abaqus. We validated the convenience of the J-Integral and adopted a mesh size to ensure the relative fluctuation of the J-integrals is below 1%. The special J-integral path (O-P-Q-O′-Q′-P′-O as illustrated in Fig. 4c) is for our calculation using a sample with $d/r = 0.8$. It can be seen that high von Mises stress locates inside the selected 'crack front' zone. The J-Integrals are then used to calculate the stress initiation intensity factor K_0 by employing the relationship of $K_0 = \sqrt{\frac{JE}{1-\nu^2}}$, and K_0 is then normalized by $\sigma_\infty\sqrt{\pi r}$ for σ_∞ being the norminal stress (the applied loading divided by the residual cross-section area).

We show in Fig. 5a the stress intensity factor (SIF) K_0 as a function of position along the crack-tip line from 'A' to 'B' for several locations of the pore, $d/r = -0.50, 0.00, 0.50, \cdots, 50$, where r = $20\mu m$ and $R/r = 80$. The stress intensity factor (SIF) K_0 maximizes in the near surface, where fatigue crack is prone to initiate. The maximum K_0 near surface is about 1.4 times greater than that of deep pores, in accordance with our experimental observations that crack primarily initiate from the subsurface of all samples. We note that there had been lots of researches regarding the influence of pores or inclusions on fatigue in polystalline materials, see Murakami et al.[6,13–17,22,46]. Murakami proposed an empirical formula $K_{Imax} \cong 0.629\sigma_\infty\sqrt{\pi\sqrt{A}}$ from experimental [6] to estimate the stress intensity factor when deeply embedded defects present, where A is the projection area of a defect under consideration. For spherical pores with diameter r, $A = \pi r^2$. Plugging it into the Murakami formula, we yield $K_{Imax} \cong 0.834\sigma_\infty\sqrt{\pi r}$. The coefficient of 0.834 agrees well with our FEM result of 0.80 (see Fig. 5a for the curves with $d/r = 5, 10, 50$). There are views suggested that in the vicinity of a corner point apparent stress intensity factors are a function of the finite element mesh and depend on the calculating method [47]. As there is no suitable definition for stress intensity factor at the corner point, and also there is no suitable element size for the point, we neglect calculations for the corner point. The results in Fig. 5a show the change of stress intensity factor approaching the corner point, which is stable when ultra-fine mesh in the proximity of the corner is adopted.

We further analyzed all fatigue fractured samples and recorded their pore size and stress amplitude. In contrast with samples with 'infinite life', we may define a fatigue threshold for BMGs in resemble of that in conventional crystalline materials. We use the maximum SIF K_0 of all fatigued samples as the threshold. It is noted that as the pore brings in an

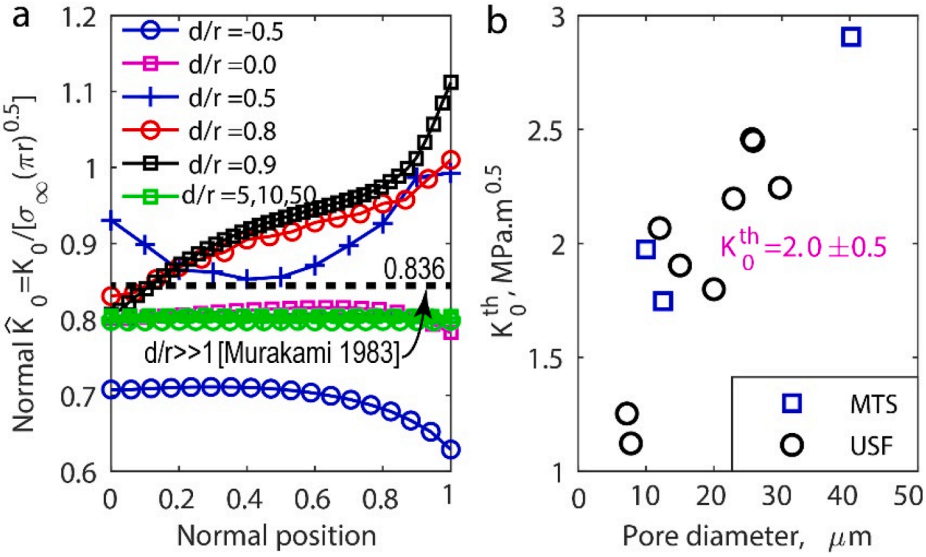

Fig. 5. Stress intensity factor K_0. (a) Normalized stress intensity factor $\widehat{K}_0$ ($\widehat{K}_0 = K_0/(\sigma_\infty\sqrt{\pi r})$) along the crack front from position "A" (0) to position "B" (1) before crack initiation; $\widehat{K}_0$ along the crack-tip line for different pore positions are shown here. (b) The threshold stress intensity factor K_0^{th} for fatigue crack initiation obtained from USF and MTS fatigued samples. An average value of $K_0^{th} = 2.0 \pm 0.5$ MPa$\sqrt{m}$ is obtained.

intrinsic length scale, mathematically K_0 is a function of pore radius, its position along the equatorial line (crack front), and the relative position of the pore d/r. The procedure is as follows: (1) we measured the pore size r and its postion d with respect to the sample edge from the fractrography of fatigued sample. (2) Using our FEM analysis on the SIF, for a pore radius r with knowing d/r, we calculate the maximum K_0 at 'B'. (3) The calculated K_0 is then the fatigue threshold of the particular pore size and location, and is defined as K_0^{th}. In Fig. 5b, we plot K_0^{th} from our tests on Vitreloy 1^{TM} metallic glass for twelve fatigued samples. The data seems to be scattering but that is typical for the value of fatigue thresholds. Nonetheless, we are able to obtain a value of $K_0^{th} = 2.0 \pm 0.5\text{MPa}\sqrt{m}$ from experiments. In previous reports, researchers had estimated the threshold on the order of $1\text{MPa}\sqrt{m}$ [38] and our approach supplies a direction experimental strategy to measure it with excellent fidelity.

3.4. Ellipse crack front

The crack front shape and its evolution for a axle or rod under fatigue loading had been an active topics during the end decades of the last century. Many works conducted FEM simulation basing on fatigue crack propagation Paris' law to predict the shape of the crack front shape, including FEM simulations [48–50] and XFEM simulations [51], two parameter and three parameter controlled ellipse arc models [52–54], stress intensity factor solutions [55], J-Integral [44], propagation laws [56]. The comprehensive review is given by Brighenti and Carpinteri [57]. To date, experimental and related calibrations researches on crack front in cylindrical samples are limited. We experimentally demonstrate, using Vitreloy 1^{TM}, so far one of the most isotropic material fit to existing linear isotropic elasticity theories, that the fatigue crack fronts resemble an ellipse arc till final rapid rupture.

In Fig. 6 we show the fatigue crack propagation and fracture front of three USF samples and three MTS samples. It is clearly shown that the fatigue crack front resembles an ellipse arc, and the loci of the ellipse crack front is at the pore center where fatigue fractgure initiates. We measure all ellipse crack front, their half short axis a and half long axis b. We show in Fig. 7a the crack propagation and the crack front profile from our experiments (solid blue lines). The half short axis a and half long axis b follows a strong correlation which is best fitted using $b = 0.61a^2 + 1.11a$, as demonstrated in Fig. 7b. Such experimental results can be meaningful guidance for further fracture mechanics analysis for isotropic solids. We further note that crack fronts tend to intersect the free surface at a critical angle, which will give rise to corner point singularity. We did not consider this special scenario in our calculations to avoid the apparent difficulty in calculations and also arisen ambiguity in defining a representative volume at the particular point.

3.5. Fatigue fracture toughness

During the last state of fatigue crack, the sample fractures quickly with very limit number of cycles. In most cases, it is regarded as brittle fracture. Based on the crack-front profile discovered present we may be able to calculate the corresponding fracture toughness of Vitreloy 1^{TM}. The mode I stress intensity factor K_I along the fracture front for both the USF and MTS samples are calculated using Abaqus J-integral method [44,45], and then the standard relationship of $K_I = \sqrt{JE/(1-\nu^2)}$ [58], where J is the caculated J-intergral [59]. As we demonstrate in Fig. 5, the stress intensity factor may vary along the elliptic arc – the crack front. We show in Fig. 8a the finite element analyses on K_I for five typical crack depths a wiith $a/2R$ ratio of 0.09, 0.12, 0.18, 0.25, and 0.34, and the elliptic long axis b is caculated using fitted equation $b = 0.61a^2 + 1.11a$, as shown in Fig. 7b. the calculated mode I stress intensity factor are further normalized by $\sigma_\infty\sqrt{\pi a}$ for σ_∞ being also the nominal stress. It is noted that there is a slight variation of K_I along the crack front curve and we take the average of K_I along the arc for the consideration that the crack front seems to propagate concurrently although at different crack-growth rate along the front. The K_{IC} and their deviation for the pesent USF and MTS test samples are shown in Fig. 8b, and an overall average of $K_{IC} = 19.7 \pm 4.6\text{MPa}\sqrt{m}$ is obtained.

It is noted that current reports on the fracture toughness are quite scattering. Gilbert et al. [28] conducted fracture toughness tests according to ASTM standard E399 on 7mm thick compact tension (CT) samples of Vitreloy 1^{TM} metallic glass, and they obtained a remarkable

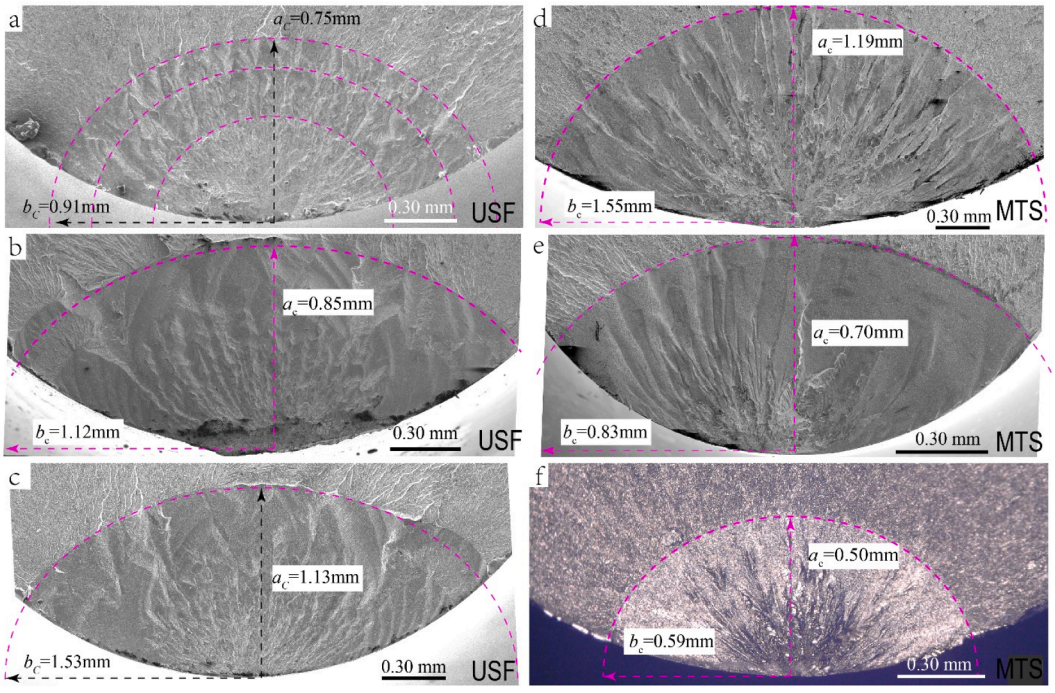

Fig. 6. Ellipse fracture crack front layouts for three typical USF (a, b and c) and three typical MTS (d–f) fatigue test samples, as marked, the typical propagation front and typical fracture front are all part ellipse arcs, and the ellipse center are all located in the near surface pore positions.

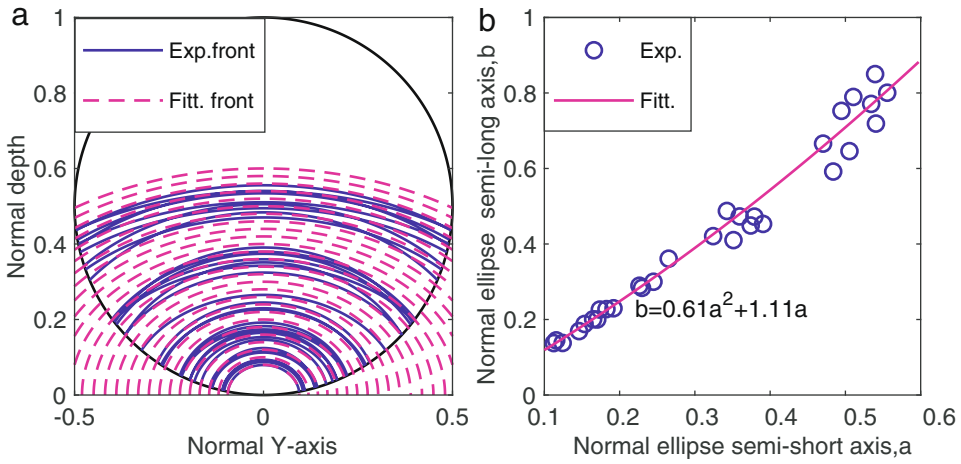

Fig. 7. Crack front profile of fatigue fracture in Vitreloy 1^{TM}. (a) Crack front profile from our experiments (solid blue lines) and quadratic fitting (dashed red lines). (b) The short and long axis correlation of elliptical crack plane during fatigue crack propagation. (For interpretation of the references to colour in this figure legend, the reader is referred to the web version of this article.)

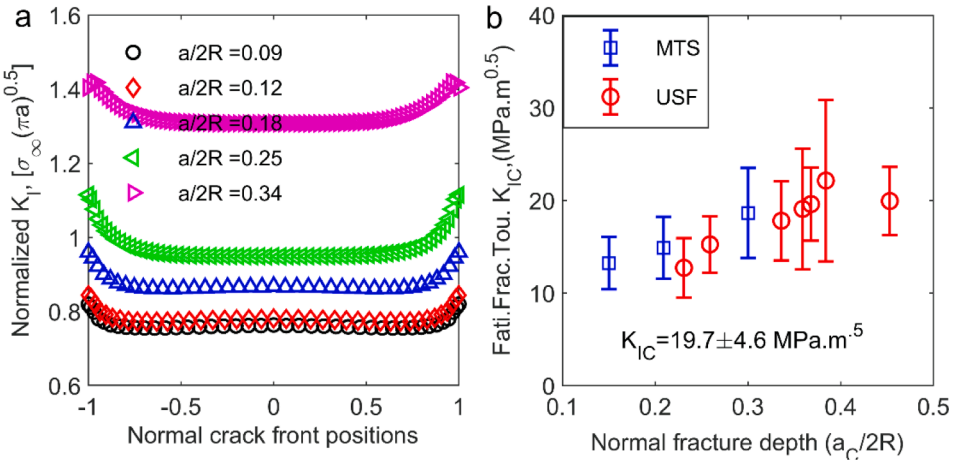

Fig. 8. Stress intensity factor and fracture toughness from fatigue fractured samples. (a) Mode I stress intensity factor K_I along a pore with different $a/2R$ ratio, 0.09, 0.12, 0.18, 0.25, and 0.34; the long axis b is calculated using $b = 0.61a^2 + 1.11a$. Normalized positions as -1, 0, and 1 correspond to the left, the apex and the right of the crack front arc. (b) The fracture toughness K_{IC} obtained from the ellipse arc of a fracture front, and we also show its standard deviation statistics from USF and MTS test specimens.

high fracture toughness of 55 65MPa$\sqrt{m}$. However, after partial or full crystallization the fracture toughness K_{IC} values drops to 1.0 1.2MPa$\sqrt{m}$. Gilbert et al. [29] conducted similar test on 4 mm thick compact tension (CT) samples and obained a fracture toughness of 30MPa$\sqrt{m}$ for Vitreloy 1^{TM}. Lowhaphandu et al. [60] conducted ASTM E399 standard fracture toughness tests on 4 mm thick samples and found that, six fatigue pre-cracked samples yielded a fracture toughness of $K_{IC} = 18.4 \pm 1.4$MPa$\sqrt{m}$. Gludovatz et al [61] conducted fracture toughness test on compact-tension and single-edge notched-bend specimens of $Zr_{52.5}Cu_{17.9}Ni_{14.6}Al_{10}Ti_5$ (Vitreloy 105^{TM}, similar with Vitreloy 1^{TM}) metallic glass with different size, and they concluded that unlike polycrystallines, the K_{IC} value of BMGs have strong dependent with the test sample size. Sun and Wang [62] in 2015 had reviewed different reports of fracture toughness which could be resulted from specimen geometry effects, compositional and internal-state, fatigue pre-cracking procedures, or a combination of these factors. The present results basing on typical cylinder geometry and similar to the pre-crack samples, agree well with the results from Lowhaphandu et al. [60] and it is also for ideally (atomic) sharp crack propagation, which is essential for real fracture toughness measurement as one tries to fulfil the requirements of ASME standard fracture tests.

4. Summary and conclusions

Fatigue endurance limit is a threshold stress amplitude under which a solid subjected to cyclic loading can sustain infinite life. Such a limit has been confirmed in ferrous materials but remains controversial in many advanced new materials, including bulk metallic glasses with superb strength. By using a combination of ultrasonic fatigue (USF) tests at 20 kHz and conventional fatigue (MTS) tests at 30 Hz for the Vitreloy 1^{TM} metallic glass (fatigue ratio $R = -1$), we obtain several interesting observations regarding fatigue fracture in Vitreloy 1^{TM}. We show from the S-N data at two frequencies from high cycle fatigue to ultra-high cycle fatigue tests that a fatigue endurance limit, which is about 320 MPa, and is only ~17% of its strength of 1900 MPa. The low fatigue endurance limit is a resultant of inevitable and intrinsic pores in this materials. We experimentally demonstrate, using Vitreloy 1^{TM}, fatigue threshold of this BMG is $K_0^{th} = 2.0 \pm 0.5$MPa$\sqrt{m}$, and its mode I fatigue fracture toughness is $K_{IC} = 18$–20 MPa$\sqrt{m}$ for atomically sharp crack, which agree well with the pre-cracked fracture toughness test results.

From our experimental observation, we see that the fatigue crack front resembles an ellipse arc. The loci of the ellipse crack front is at the pore center where fatigue fracture initiates, and their half short axis a and half long axis b follows a strong correlation captured by $b = 0.61a^2 + 1.11a$. Given metallic glass can be regarded as one of the most isotropic material at the continuum level, such observations is best suited for isotropic elasticity theories, which can be employed for further fracture mechanics analysis.

As previous explorations on fatigue endurance limit often followed

the traditional 'infinite life' assumption at loading cycles up to $N_{f0} = 10^7$, it is not an unabigious proof the real existence of such an FEL. The combination of conventional fatigue tests using MTS machines and ultrasonic fatigue (USF) facility helped realizing the fatigue cycles ranging from 10^4 to 10^9. More importantly, we see clearly from both 'infinite life' cycles 10^7 and 10^9 that there is an FEL at the same stress level. Such an experimental endeavor makes the fatigue performance evaluation of BMGs engineering practical.

Declaration of Competing Interest

The authors declare that they have no known competing financial interests or personal relationships that could have appeared to influence the work reported in this paper.

Acknowledgements

The authors are grateful to Prof. Yuan Gao from Tsinghua University for kind discussing of J-Integral caculation using ABAQUS. The authors acknowledge support from National Natural Science Foundation of China (NSFC) Basic Science Center for "Multiscale Problems in Nonlinear Mechanics" (Grant 11988102), as well as NSFC Grants 11790291 and 11802308; the Strategic Priority Research Program of the Chinese Academy of Sciences (CAS) (Grant XDB22020200), and CAS Center for Excellence in Complex System Mechanics.

References

[1] ASM International Handbook Committee, ASM Handbook, Fatigue and Fracture, ASM International, Materials Park, Ohio, 1996.
[2] Schijve J. Fatigue of structures and materials in the 20th century and the state of the art. Int J Fatigue 2003;25(8):679–702.
[3] Chan KS. Roles of microstructure in fatigue crack initiation. Int J Fatigue 2010;32(9):1428–47.
[4] Pyttel B, Schwerdt D, Berger C. Very high cycle fatigue - Is there a fatigue limit? Int J Fatigue 2011;33(1):49–58.
[5] Tanaka K, Mura T. A dislocation model for fatigue crack initiation. J Appl Mech-Trans ASME 1981;48(1):97–103.
[6] Murakami Y, Endo M. Quantitative-evaluation of fatigue-strength of metals containing various small defects or cracks. Eng Fract Mech 1983;17(1):1–15.
[7] La Rosa G, Risitano A. Thermographic methodology for rapid determination of the fatigue limit of materials and mechanical components. Int J Fatigue 2000;22(1):65–73.
[8] Wang XG, Crupi V, Jiang C, Guglielmino E. Quantitative Thermographic Methodology for fatigue life assessment in a multiscale energy dissipation framework. Int J Fatigue 2015;81:249–56.
[9] Wang QY, Bathias C, Kawagoishi N, Chen Q. Effect of inclusion on subsurface crack initiation and gigacycle fatigue strength. Int J Fatigue 2002;24(12):1269–74.
[10] Billaudeau T, Nadot Y, Bezine G. Multiaxial fatigue limit for defective materials: mechanisms and experiments. Acta Mater 2004;52(13):3911–20.
[11] Sangid MD, Maier HJ, Sehitoglu H. A physically based fatigue model for prediction of crack initiation from persistent slip bands in polycrystals. Acta Mater 2011;59(1):328–41.
[12] Sun C, Song Q, Zhou L, Liu J, Wang Y, Wu X, et al. The formation of discontinuous gradient regimes during crack initiation in high strength steels under very high cycle fatigue. Int J Fatigue 2019;124:483–92.
[13] Murakami Y, Endo M. Effects of defects, inclusions and inhomogeneities on fatigue-strength. Int J Fatigue 1994;16(3):163–82.
[14] Murakami Y, Nomoto T, Ueda T. Factors influencing the mechanism of superlong fatigue failure in steels. Fatigue Fract Eng Mater Struct 1999;22(7):581–90.
[15] Zerbst U, Madia M, Klinger C, Bettge D, Murakami Y. Defects as a root cause of fatigue failure of metallic components. I: Basic aspects. Eng Fail Anal 2019;97:777–92.
[16] Zerbst U, Madia M, Klinger C, Bettge D, Murakami Y. Defects as a root cause of fatigue failure of metallic components. III: Cavities, dents, corrosion pits, scratches. Eng Fail Anal 2019;97:759–76.
[17] Zerbst U, Madia M, Klinger C, Bettge D, Murakami Y. Defects as a root cause of fatigue failure of metallic components. II: Non-metallic inclusions. Eng Fail Anal 2019;98:228–39.
[18] Przybyla CP, Musinski WD, Castelluccio GM, McDowell DL. Microstructure-sensitive HCF and VHCF simulations. Int J Fatigue 2013;57:9–27.
[19] Papuga J. A survey on evaluating the fatigue limit under multiaxial loading. Int J Fatigue 2011;33(2):153–65.
[20] Suresh S. Fatigue of Materials. 1st ed. New York: Cambridge University Press; 1998.
[21] Kruzic JJ. Predicting fatigue failures. Science 2009;325(5937):156–8.
[22] Murakami Y. Material defects as the basis of fatigue design. Int J Fatigue 2012;41:2–10.
[23] Chen M. A brief overview of bulk metallic glasses. NPG Asia Mater 2011;3:82–90.
[24] Inoue A. Stabilization of metallic supercooled liquid and bulk amorphous alloys. Acta Mater 2000;48(1):279–306.
[25] Ketov SV, Sun YH, Nachum S, Lu Z, Checchi A, Beraldin AR, et al. Rejuvenation of metallic glasses by non-affine thermal strain. Nature 2015;524(7564):200–3.
[26] Schuh CA, Hufnagel TC, Ramamurty U. Overview No.144 - Mechanical behavior of amorphous alloys. Acta Mater 2007;55(12):4067–109.
[27] Wagner H, Bedorf D, Kuechemann S, Schwabe M, Zhang B, Arnold W, et al. Local elastic properties of a metallic glass. Nat Mater 2011;10(6):439–42.
[28] Gilbert CJ, Ritchie RO, Johnson WL. Fracture toughness and fatigue-crack propagation in a Zr-Ti-Ni-Cu-Be bulk metallic glass. Appl Phys Lett 1997;71(4):476–8.
[29] Gilbert CJ, Schroeder V, Ritchie RO. Mechanisms for fracture and fatigue-crack propagation in a bulk metallic glass, Metallurgical and Materials Transactions a-Physical Metallurgy and Materials. Science 1999;30(7):1739–53.
[30] Menzel BC, Dauskardt RH. Stress-life fatigue behavior of a Zr-based bulk metallic glass. Acta Mater 2006;54(4):935–43.
[31] Yue Y, Wang R, Ma DQ, Tian JF, Zhang XY, Jing Q, et al. Fatigue behavior of a Zr-based bulk metallic glass under uniaxial tension-tension and three-point bending loading mode. Intermetallics 2015;60:86–91.
[32] Wang XD, Liu P, Zhu ZW, Zhang HF, Ren XC. High fatigue endurance limit of a Ti-based metallic glass. Intermetallics 2020;119.
[33] Fujita K, Zhang W, Shen B, Amiya K, Ma CL, Nishiyama N. Fatigue properties in high strength bulk metallic glasses. Intermetallics 2012;30:12–8.
[34] Yokoyama Y, Liaw PK, Nishijima M, Hiraga K, Buchanan RA, Inoue A. Fatigue-strength enhancement of cast Zr50Cu40Al10 glassy alloys. Mater Trans 2006;47(5):1286–93.
[35] Wang CC, Mao YW, Shan ZW, Dao M, Li J, Sun J, et al. Real-time, high-resolution study of nanocrystallization and fatigue cracking in a cyclically strained metallic glass. PNAS 2013;110(49):19725–30.
[36] Cameron KK, Dauskardt RH. Fatigue damage in bulk metallic glass I: Simulation. Scr Mater 2006;54(3):349–53.
[37] Sha Z, Wong WH, Pei Q, Branicio PS, Liu Z, Wang T, et al. Atomistic origin of size effects in fatigue behavior of metallic glasses. J Mech Phys Solids 2017;104:84–95.
[38] Jia H, Wang G, Chen S, Gao Y, Li W, Liaw PK. Fatigue and fracture behavior of bulk metallic glasses and their composites. Prog Mater Sci 2018;98:168–248.
[39] Wang GY, Liaw PK, Peker A, Yang B, Benson ML, Yuan W, et al. Fatigue behavior of Zr-Ti-Ni-Cu-Be bulk-metallic glasses. Intermetallics 2005;13(3–4):429–35.
[40] Launey ME, Busch R, Kruzic JJ. Influence of structural relaxation on the fatigue behavior of a Zr41.25Ti13.75Ni10CU12.5Be22.5 bulk amorphous alloy. Scr Mater 2006;54(3):483–7.
[41] Menzel BC, Dauskardt RH. Fatigue damage initiation and growth from artificial defects in Zr-based metallic glass. Acta Mater 2008;56(13):2955–65.
[42] Zhou X, Li X, Chen C. Atomistic mechanisms of fatigue in nanotwinned metals. Acta Mater 2015;99:77–86.
[43] Sha Z, Teng Y, Poh LH, Pei Q, Xing G, Gao H. Notch strengthening in nanoscale metallic glasses. Acta Mater 2019;169:147–54.
[44] Courtin S, Gardin C, Bezine G, Hamouda HB. Advantages of the J-integral approach for calculating stress intensity factors when using the commercial finite element software ABAQUS. Eng Fract Mech 2005;72(14):2174–85.
[45] ABAQUS (2014) 'ABAQUS 6.14 Analysis User's Guide: 11.4 Fracture Mechanics', Dassault Systèmes Simulia Corp., Providence, RI, USA.
[46] Murakami Y. Metal fatigue: effects of small defects and nonmetallic inclusions. Second Ed. Academic Press & Elsevier; 2019.
[47] Pook LP. A 50-year retrospective review of three-dimensional effects at cracks and sharp notches. Fatigue Fract Eng Mater Struct 2013;36(8):699–723.
[48] Gilchrist MD, Smith RA. Finite-element modeling of fatigue crack shapes. Fatigue Fract Eng Mater Struct 1991;14(6):617–26.
[49] Lin XB, Smith RA. Shape growth simulation of surface cracks in tension fatigued round bars. Int J Fatigue 1997;19(6):461–9.
[50] Lin XB, Smith RA. Shape evolution of surface cracks in fatigued round bars with a semicircular circumferential notch. Int J Fatigue 1999;21(9):965–73.
[51] Bergara A, Dorado JI, Martin-Meizoso A, Martinez-Esnaola JM. Fatigue crack propagation in complex stress fields: Experiments and numerical simulations using the Extended Finite Element Method XFEM. Int J Fatigue 2017;103:112–21.
[52] Carpinteri A. Shape change of surface cracks in round bars under cyclic axial loading. Int J Fatigue 1993;15(1):21–6.
[53] Carpinteri A, Brighenti R. Part-through cracks in round bars under cyclic combined axial and bending loading. Int J Fatigue 1996;18(1):33–9.
[54] Couroneau N, Royer J. Simplified model for the fatigue growth analysis of surface cracks in round bars under mode I. Int J Fatigue 1998;20(10):711–8.
[55] Shin CS, Cai CQ. Experimental and finite element analyses on stress intensity factors of an elliptical surface crack in a circular shaft under tension and bending. Int J Fract 2004;129(3):239–64.
[56] Pugno N, Ciavarella M, Cornetti P, Carpinteri A. A generalized Paris' law for fatigue crack growth. J Mech Phys Solids 2006;54(7):1333–49.
[57] Brighenti R, Carpinteri A. Surface cracks in fatigued structural components: a review. Fatigue Fract Eng Mater Struct 2013;36(12):1209–22.
[58] Zhu XK, Joyce JA. Review of fracture toughness (G, K, J, CTOD, CTOA) testing and standardization. Eng Fract Mech 2012;85:1–46.
[59] Rice JR. A path independent integral and approximate analysis of strain concentration by notches and cracks. J Appl Mech 1968;35(2):379–86.

[60] Lowhaphandu P, Lewandowski JJ. Fracture toughness and notched toughness of bulk amorphous alloy: Zr-Ti-Ni-Cu-Be. Scr Mater 1998;38(12):1811–7.
[61] Gludovatz B, Naleway SE, Ritchie RO, Kruzic JJ. Size-dependent fracture toughness of bulk metallic glasses. Acta Mater 2014;70:198–207.
[62] Sun BA, Wang WH. The fracture of bulk metallic glasses. Prog Mater Sci 2015;74:211–307.